Aerosol Characterization of the Stratospheric Plume From the Volcanic Eruption at Hunga Tonga 15 January 2022

Corinna Kloss, Pasquale Sellitto, Jean-Baptiste Renard, Alexandre Baron, Nelson Bègue, Bernard Legras, Gwenaël Berthet, Emmanuel Briaud, Elisa Carboni, Clair Duchamp, et al.

AGU ADVANCING EARTH AND SPACE SCIENCE

Geophysical Research Letters®

RESEARCH LETTER
10.1029/2022GL099394

Key Points:

- Predominant particle size range of <1 μm within the stratospheric aerosol plume of the Hunga Tonga eruption
- Optically absorbing particles within the plume for particles <0.5 μm point to fractured, very small ash particles
- Mostly optically semi-transparent particles, for particle sizes between 0.5 and 1.0 μm result from small sulfur coated ash particles

Supporting Information:

Supporting Information may be found in the online version of this article.

Correspondence to:

C. Kloss,
corinna.kloss@cnrs-orleans.fr

Citation:

Kloss, C., Sellitto, P., Renard, J.-B., Baron, A., Bègue, N., Legras, B., et al. (2022). Aerosol characterization of the stratospheric plume from the volcanic eruption at Hunga Tonga 15 January 2022. *Geophysical Research Letters*, *49*, e2022GL099394. https://doi.org/10.1029/2022GL099394

Received 7 MAY 2022
Accepted 24 JUL 2022

Aerosol Characterization of the Stratospheric Plume From the Volcanic Eruption at Hunga Tonga 15 January 2022

Corinna Kloss[1], Pasquale Sellitto[2,3], Jean-Baptiste Renard[1], Alexandre Baron[4], Nelson Bègue[4], Bernard Legras[5], Gwenaël Berthet[1], Emmanuel Briaud[1], Elisa Carboni[6], Clair Duchamp[5], Valentin Duflot[4], Patrick Jacquet[1], Nicolas Marquestaut[7], Jean-Marc Metzger[7], Guillaume Payen[7], Marion Ranaivombola[4], Tjarda Roberts[1], Richard Siddans[6], and Fabrice Jégou[1]

[1]Laboratoire de Physique et Chimie de l'Environnement et de l'Espace (LPC2E), CNRS/Université d'Orléans, UMR 7328, Orléans, France, [2]Université Paris Est Créteil and Université de Paris-Cité, CNRS/Laboratoire Interuniversitaire des Systèmes Atmosphériques (LISA), Institut Pierre Simon Laplace (IPSL), Créteil, France, [3]Istituto Nazionale di Geofisica e Vulcanologia, Osservatorio Etneo, Catania, Italy, [4]Laboratoire de l'Atmosphère et des Cyclones (LACy), CNRS/Université de la Réunion/Météo-France, UMR 8105, Saint-Denis, France, [5]Laboratoire de Météorologie Dynamique, ENS-PSL/ Sorbonne Université/ École Polytechnique, UMR CNRS, Paris, France, [6]Rutherford Appleton Laboratory, UK Research and Innovation, Science and Technology Facilities Council, Chilton, UK, [7]Observatoire des Sciences de l'Univers de La Réunion (OSUR), CNRS/Université de La Réunion/Météo-France), UAR 3365, Saint-Denis, France

Abstract Following the Hunga Tonga eruption (20.6°S, 175.4°W, mid-January 2022), we present a balloon-borne characterization of the stratospheric aerosol plume one week after its injection (on 23 and 26 January 2022, La Réunion island at 21.1°S, 55.3°E). Satellite observations show that flight (a) took place during the overpass of a denser plume of sulfate aerosols (SA) compared to a more diluted plume during flight. (b) Observations show that the sampled plumes (at around 22, 25 and 19 km altitude, respectively) consist exclusively of very small particles (with radius <1 μm). Particles with radii between 0.5 and 1.0 μm show optically transparent features pointing to predominant SA. Particles with radii below 0.5 μm are partly absorbing, which could point to small sulfate coated ash particles, a feature not identified with space-borne observations. This shows that in situ observations are necessary to fully characterize the microphysical properties of the plumes tracked by space-borne instruments.

Plain Language Summary The Hunga Tonga-Hunga Ha'apai volcano (at 20.6°S, 175.4°W) erupted on 13 and 15 January 2022 with injection of gases and aerosols up to 55 km altitude. Here, we present a study based on in situ aerosol observations on weather balloons on La Réunion (21.1°S, 55.3°E) within the injected Hunga Tonga aerosol plume one week after the eruption (23 and 26 January 2022). With respective satellite observations, we show that the first measurement flight took place during the overpass of a denser aerosol plume compared to the second flight. We find that the plume exhibits only small particles <1 μm, mainly consisting of sulfate aerosols (for particles between 0.5 and 1 μm in size) and an absorbing component for very small particles (<0.5 μm), possibly pointing to small ash particles coated by sulfur. This letter "absorbing" feature is a unique contribution brought by in situ measurements that fills a gap left by space-borne instruments.

1. Introduction

The Hunga Tonga-Hunga Ha'apai (hereafter referred to as Hunga Tonga) volcano (20.57°S, 175.38°W) started an eruptive phase on 20 December 2021, with gas, steam and ash plumes periodically injected at around 12 km altitude. In mid-January larger eruptive events occurred on 13 and 15 January e.g., Yuen et al. (2022), Carr et al. (2022). The sub-aerial eruption on 13 January started at 15:20 UTC, injected plumes into the stratosphere that were observed at altitudes as high as 20 km, with an estimated sulfur dioxide (SO_2) burden of 0.05 Tg (Witze, 2022). A larger, submarine, explosive eruption started on 15/01 at 04:02 UTC (Yuen et al., 2022), with an estimated SO_2 burden of 0.4–0.5 Tg (Witze, 2022). The CALIPSO-CALIOP (The Cloud-Aerosol Lidar and Infrared Pathfinder Satellite Observation) space LiDAR observed an aerosol plume with depolarizing properties at altitude of 38 km, on 15/01 (Sellitto et al., 2022). The plume is composed of sub-mironic sulfate particles, whereas no residual signature of ash is found starting a few hours after the injection with HIMAWARI and CALIOP observations (Legras et al., 2022). Stereoscopic geostationary observations suggest plume top altitudes

of 50–55 km at 04:30 UTC (Carr et al., 2022; Proud et al., 2022) building a record altitude of any observed volcanic plume.

The extraordinary nature of this eruption in terms of explosivity and subsequent injection altitude in the stratosphere, as well as large aerosol and water vapor in-plume contents (Sellitto et al., 2022; Zhu et al., 2022), have immediately triggered vivid discussions and scientific exchange within the atmospheric community. We reactively organized a fast in situ measurement campaign for high-resolution aerosol observations within the injected plume to characterize the optical and microphysical composition of the plume. Here, we present in situ observations on the aerosol concentration and size distribution and corresponding analysis of the optical and microphysical properties of the aerosols within the stratospheric Hunga Tonga plume with the Light Optical Aerosol Counter (LOAC) on two balloon flights from Observatoire de Physique de l'Atmosphère de la Réunion (OPAR, 21.1°S and 55.3°E) on 23 and 26 January. At almost the same latitude and downwind of the Hunga Tonga plume's dispersion, OPAR is the ideal place for such early aerosol plume in situ investigations.

2. Methods

2.1. The LOAC Balloon-Borne Optical Counter

The Light Optical Aerosol Counter (LOAC) is an optical counter instrument that can be operated on weather balloons for observations in the stratosphere (Renard et al., 2016; Renard, Michoud, & Giacomoni, 2020), with substantial improvements throughout its existence). For the described measurement flights, we used version 1.5 of the LOAC instrument with an improved optical chamber and sensitivity with a more powerful laser source compared to the previous version. LOAC provides measurements every 10 seconds. For an increased signal-to-noise ratio, data are binned over an integration time of 20s.

We use in situ measurement from LOAC on weather balloon flights from 23 January (20:04–21:35 UTC) and 26 January (17:24–19:54 UTC) at the Maïdo Observatory at La Réunion (21.1°S, 55.3°E). The LOAC instrument measures size-resolved aerosol concentration for particle sizes between 0.2 µm and ∼30 mm diameter (laser wavelength at 650 nm) distributed on 19 size classes. The detection uncertainty for the size attribution is around 10% for particles >2 µm. For smaller particles, the size determination is within the calibration error bars, that is, 5% for particles between 0.7 and 1 µm and around ±0.025 µm for particles smaller than 0.6 µm (if more than 400 particles are detected for each size class). Some uncertainties remain concerning the size distribution for non-spherical particles as discussed in (Renard et al., 2016). One outstanding feature of LOAC compared to other comparable instruments is the detection of scattered light at two angles (15 and 65° respective to the laser beam). This allows for a partial characterization of the light absorbing properties and thus the typology of the observed aerosols (i.e., distinction between optically absorbing, semi-transparent and transparent solid particles, liquid, ice particles (Renard et al., 2016). Aerosol extinction values stem from the conversion from measured aerosol concentration for size classes higher than 0.2 µm using Mie scattering theory and an estimate of the refractive index coming from the typology determination. A schematic diagram of the LOAC measurement principle is provided (Figure S1 in Supporting Information S1).

2.2. LiDAR Observations at the Maïdo Observatory

LiDAR data used in this study are derived from observations conducted at the Maïdo Observatory, one of the three observation sites of the Atmospheric Physics Observatory of La Réunion (OPAR) located on Reunion Island (21.1°S, 55.3°E). The Maïdo Observatory is a permanent station, situated at 2160 m above mean sea level, for long term atmospheric observations (Baray et al., 2013). The used LiDAR system is the aerosol wing of the LIO3T (Duflot et al., 2017). The aerosol optical properties are retrieved following the Rayleigh slope method presented in Chazette et al. (1995). With a significant aerosol load between aerosol-free layers, it allows for conclusions on the aerosol optical thickness (AOT) of the plume. This constraint, as an input of an iterative Klett method (Klett, 1985) for the LiDAR inversion, enables to assess both the aerosol extinction coefficient and an average LiDAR ratio of the aerosol layer. The LiDAR ratio is the ratio of the extinction-to-backscatter coefficient and gives indications on some microphysical properties of the observed aerosols. According to Dieudonné et al. (2015) only the Lidar Ratios obtained during phases of aerosol extinction observation >0.02 km^{-1} are presented. The final temporal and vertical resolutions of the presented profiles are 5 min and 50 m, respectively. Presented observations are sensitive for aerosol extinction values above 10^{-4} km^{-1}.

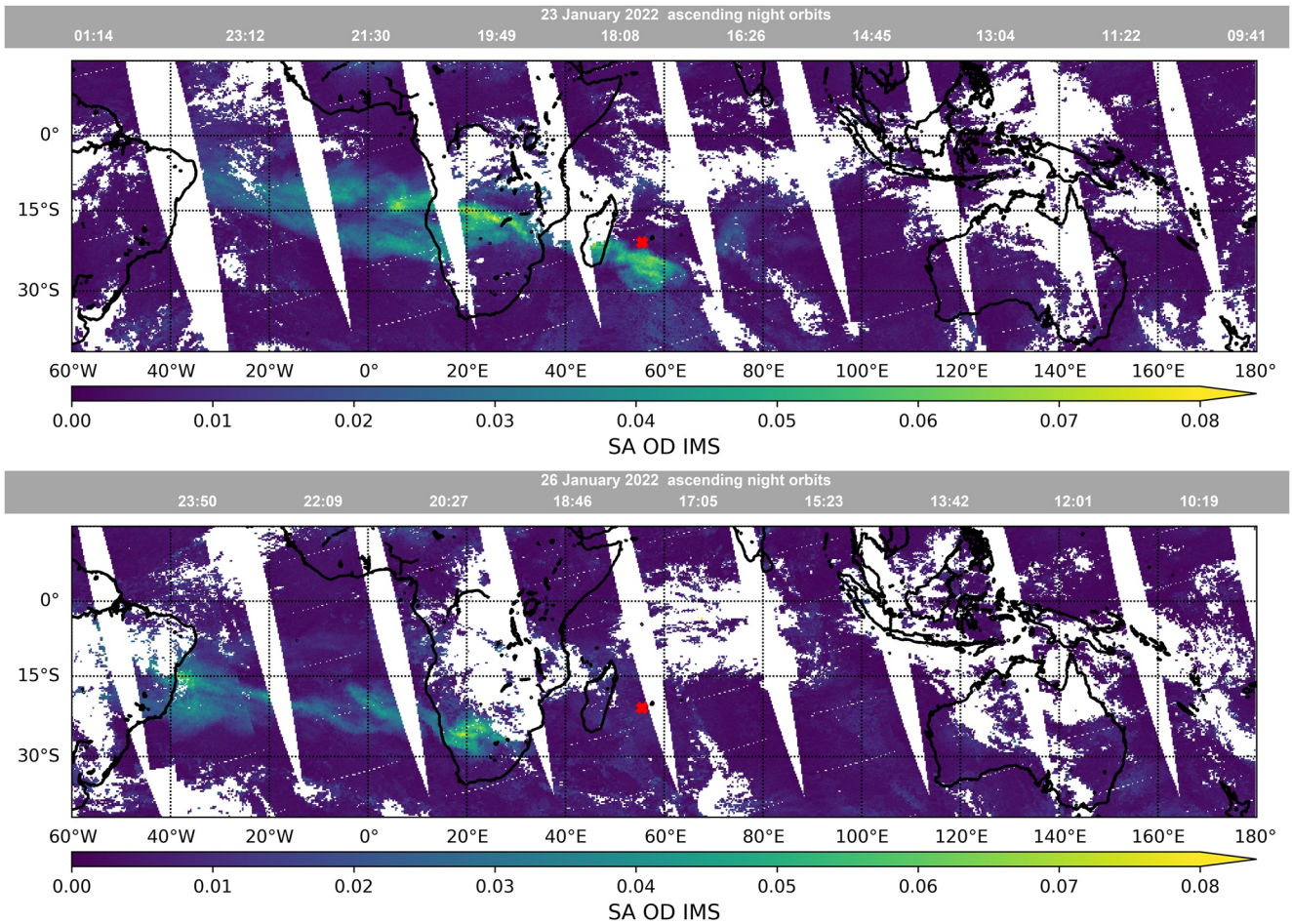

Figure 1. Infra-red/Microwave Sounder/Infrared Atmospheric Sounding Interferometer sulfate aerosols (IMS/IASI SA) optical depth observations with the respective timestamp of equator crossing in UTC (a) on 23 January and (b) on 26 January. The red cross shows the location of Light Optical Aerosol Counter measurement flights at La Réunion. Areas of no measurements and clouds are indicated in white.

2.3. IMS Sulfate Aerosols Speciation and Retrieval

The Rutherford Appleton Laboratory (RAL) Infra-red/Microwave Sounder (IMS) retrieval core scheme Siddans (2019) uses an optimal estimation (OE) spectral fitting procedure to retrieve atmospheric and surface parameters jointly from co-located measurements by Infrared Atmospheric Sounding Interferometer (IASI), Advanced Microwave Sounding Unit (AMSU) and Microwave Humidity Sounder (MHS) on MetOp spacecraft series, using RTTOV 12 (Radiative Transfer for TOVS) (Saunders et al., 2017) as the forward radiative transfer model. The use of RTTOV12 enables the retrieval of volcanic-specific aerosols (sulfate aerosol: SA) and trace gases (SO_2). The present paper uses IMS SA observations from its near-real time implementation (images can be viewed here: http://rsg.rl.ac.uk/vistool). The IMS scheme retrieves the optical depth of the SA at ~1200 cm^{-1} (the peak of the mid-infrared extinction cross section, Sellitto and Legras (2016), assuming a Gaussian extinction coefficient profile shape peaking at 20 km altitude, with 2 km full-width-half-maximum. The bulk of the spectroscopic information on SA, in the IMS scheme, thus comes from the IASI Fourier transform spectrometer (Clerbaux et al., 2009), thus we will refer to these observations as IMS/IASI in the following.

3. Results

3.1. Transport of the Hunga Tonga Plume Above La Réunion Island

To bring LOAC in situ observations in the larger scale context of the transported Hunga Tonga plume, we show the horizontal plume distribution with IMS SA optical depth observations in Figure 1. The first dispersion,

removal of larger ash particles and rapid formation of SA has been shown by Sellitto et al. (2022), with the HIMAWARI Ash RGB recipe and CALIOP observations. An animation of MSG-1 brightness temperature observations (Da, 2015) with the Eumetrain RGB recipe (Eumetrain, 2020) is shown in (Movie S1 and Text S1 in Supporting Information S1, respectively) for an overview of the subsequent transport of the volcanic plume over the southern Indian Ocean. The RGB recipe allows for differentiations between water and ice clouds (grayish and shades of brown), ash (shades of red) and SO_2 and SA (shades of bright green). The spectral signatures of SO_2 and SA superpose in the spectral range covered by the RGB recipe and they cannot be readily disentangled without complementary information, as provided in Sellitto et al. (2017). In this case, greenish plumes are most likely an indication of SA-dominated plumes (Sellitto et al., 2022). The MSG-1 observations show a dense volcanic SA plume above La Réunion, starting from 21 January and clearly visible until 23 January. During the night of the first LOAC observations (23 January, 20:04–21:35 UTC) the bulk SA plume had already moved to the South-West. The RGB MSG-1 analysis does not reveal a clear signature of transported ash from the Hunga Tonga eruption. However, the brightness temperature RGB retrieval is only sensitive to relatively high concentrations of ash or SA; low concentrations will therefore not clearly appear in the respective color on the map.

For a more quantitative analysis of the plume, Figure 1 shows the horizontal distribution of the SA optical depth from IMS/IASI on 23 January (Figure 1a) and 26 January (Figure 1b), close in time to LOAC measurements during the night time overpass (at La Réunion at around 18:00 UTC, compared to LOAC observations 20:04–21:35 UTC for 23 January and 17:24–19:54 UTC for 26 January). Consistently with what is observed with MSG-1 for SO_2/SA, IMS/IASI measurements suggest that the flight on 23 January took place when a denser plume of SA was transported over La Réunion. Observations on 26 January indicate a more diluted phase of the plume overpassing the island.

Values of the thermal infrared SA optical depth as large as 0.05 are found for 23 January, pointing at a dense SA plume.The vertical aerosol extinction distribution of the aerosol plume at La Réunion, from the ground-based LIO3T observations at the Maïdo Observatory, is shown on the left side in Figure 2. These remote sensing observations are taken around the measurement time frame of LOAC in situ observations. Respective LOAC aerosol extinction observations at 532 nm (wavelength chosen according to LiDAR observations), observed during the indicated time frame (20:04–21:35 UTC), are shown on the right side (and in Figure S2 in Supporting Information S1). On 23 January at 20:04–21:35 UTC LOAC observations (Figure 2a, right side and Figure S2 in Supporting Information S1) identify two main plume layers at around 22.6 and 24.9 km altitude, with peak values up to ∼4 10^{-3} km^{-1}. The LIO3T time series shows that LOAC observations were taken right before the arrival of a much denser section of the plume. With an average ascending speed of the balloon of 6 m/s in the stratosphere and a counting integration time of 20 s only a few measurement points originate from the plume. Peak aerosol extinction values between 22 and 23 km altitude from LIO3T observations during LOAC observations (∼15 10^{-3} km^{-1}, with a LiDAR uncertainty of around 25% at the plume's altitude) exceed LOAC aerosol extinction values (∼3 10^{-3} km^{-1}) by a factor of 5. Multiple factors contribute to this observed difference:

1. With an average ascending speed of the balloon of 6 m/s in the stratosphere and a counting integration time of 20 s only a few measurement points originate from the plume.
2. LOAC observations do not consider particles with diameters below 200 nm and therefore represent a lower limit of the sampled plume. However, lab experiments show that the contribution of small particles (<200 nm) to the respective Aerosol extinction values cannot account for more than that of larger particles (>200 nm). Therefore, the respective underestimation in Aerosol extinction remains well below a factor of 2.
3. LIO3T observations show the heterogeneous nature of the plume and similar extinction values compared to LOAC measurements have been observed within 2 hr of the flight. At the altitude of the plume (at ∼22.5 km), LOAC and LIO3T observations were 15.5 km apart and the plume speed was at around 15 m/s. This is expected to be the main reason for the visible discrepancy.

During the time of the LOAC observations, LIO3T data do not show aerosol enhancements at 25 km altitude (at 25 km altitude LOAC was flying around 12 km further North compared to LIO3T observations). However, 4 hr prior to LOAC observations a strong plume signal was observed at 25 km altitude for several hours to days (Figure 2, LIO3T results and longer time series will be published in more detail by Baron et al.). Furthermore, OMPS observations (Figure S4a in Supporting Information S1) show the clear presence of an aerosol plume above La Réunion at around 10 UTC up to ∼27 km altitude, with peak values at ∼25 km. The respective stratospheric Aerosol Optical Depth of 0.12 (see Figure S4b in Supporting Information S1) is significantly larger than

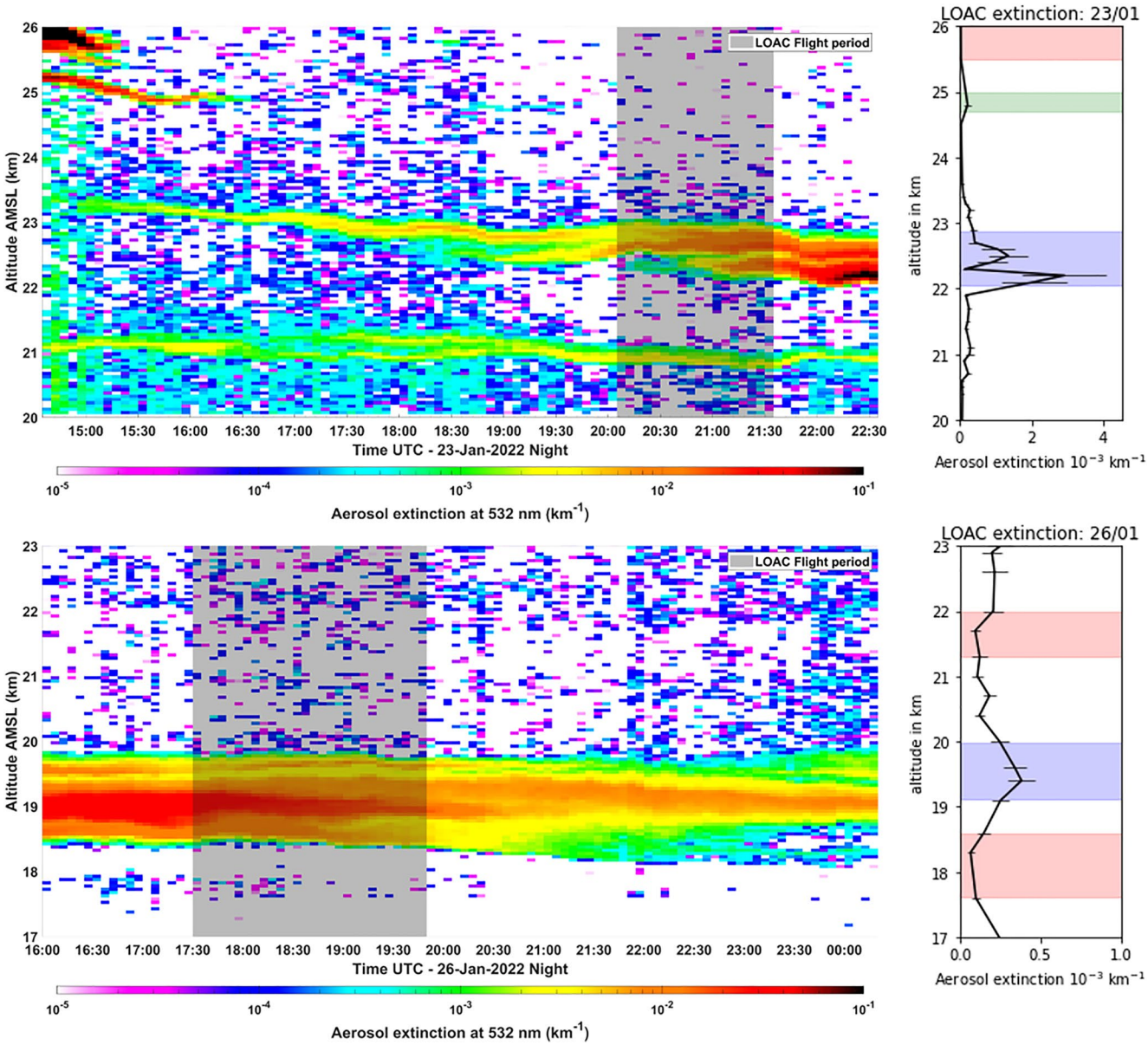

Figure 2. (left) LIO3T aerosol observations at Observatoire de Physique de l'Atmosphère de la Réunion at 532 nm wavelength for (a) 23 January and (b) 26 January. The gray shaded blocks represent the timing of the Light Optical Aerosol Counter (LOAC) in situ observations. (right) Equivalent aerosol extinction at 532 nm, retrieved from LOAC aerosol concentration in situ observations with respective error bars. Horizontal shaded areas (also shown in Figure S2 in Supporting Information S1) define altitude ranges used for further analysis (red: above/below plume, blue and green: in-plume).

LIO3T integrated optical depth observations, probably because of dense plume sections at lower stratospheric altitudes which are observed by OMPS but not by the ground LIO3T. The plume's evolution between the OMPS overpass and LOAC observations on 23 January is presented in Figures S4c and S4d in Supporting Information S1, respectively (light green shaded area). A LiDAR ratio of 68 ± 18 is observed within the peak aerosol plume. This is similar to what has previously been observed for volcanic plumes at 532 nm (Prata et al., 2017), but cannot be used to rule out the possible presence of ash, especially if diluted.

On 26 January 17:24–19:54 UTC, LOAC peak aerosol extinction values were observed at around 19.5 km altitude, with peak values at 0.4 10^{-3} km^{-1}. LIO3T observations show peak aerosol extinction values of up to 40 10^{-3} km^{-1} (around 100 times higher than LOAC observations), with a LiDAR uncertainty of about 50% at the plume altitude (18–20 km). From the LIO3T time series, it becomes evident that the LOAC time frame took place

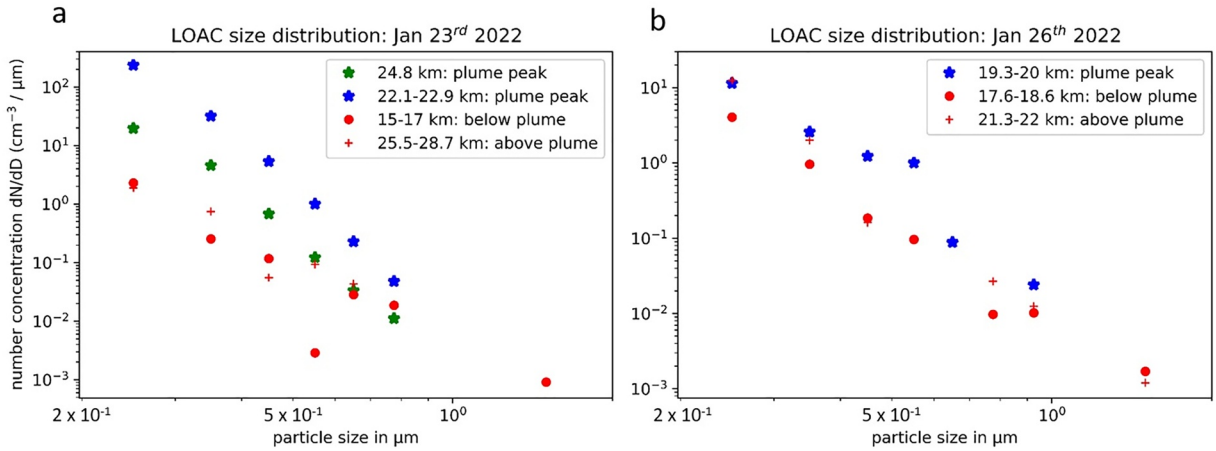

Figure 3. Observed aerosol size distribution at the identified aerosol plume heights as identified in Figure 1 and below the aerosol plume for the Light Optical Aerosol Counter (LOAC) measurements from (a) 23 January and (b) 26 January. Measurement uncertainties in size attribution and concentration are detailed in Renard et al. (2016).

during the end phase of the plume (peak phase) overpass at La Réunion. Starting from 2 hr after the flight, LIO3T observations show a patchy and fast dissolving vertical structure of the plume. With a balloon ascending speed of 6 m/s, a horizontal plume speed of ∼13 m/s and a distance of ∼20 km between in situ and LIO3T observations, it is likely that LOAC measurements missed the bulk of the plume in terms of aerosol extinction. However, the slightly increased aerosol extinction values at the plume altitude level (as observed by LIO3T) and the clearly distinguished size distribution and typology analysis give confidence that LOAC sampled particles of the respective aerosol plume. CALIOP aerosol backscatter data capture part of the same plume around 15° further West 3 hr after LOAC observations at the same altitude range (see Figure S5 in Supporting Information S1).

3.2. Characterization of the Plume's Microphysical Properties With in Situ Observations

Based on the general consistency of LOAC and LIO3T observations at La Réunion, we exploit the LOAC observations to derive the optical and microphysical properties of the Hunga Tonga plume. Aerosol size distribution observations from the two LOAC flights within and below the aerosol plume (as defined in Figure 2, right side and in Figure S2 in Supporting Information S1) are presented in Figure 3. Observed number concentrations for the two peak altitudes at 22 and 25 km on 23 January exceed aerosol background concentrations at 20 km altitude by a factor of 10–40. The observed size distribution of the background aerosol is comparable to background conditions observed during previous LOAC flights (e.g., Renard, Berthet, et al. (2020)). Size distribution observations within the aerosol plume are in the same order of those observed in other volcanic plumes (e.g., after the Calbuco eruption in 2015, Bègue et al. (2017)). One highlight result of LOAC observations is the clear identification of the upper limit aerosol size range within the Hunga Tonga plume. For the Pinatubo eruption (1991), for example, a coarse mode of aerosol peak concentration for particles with radii >1 µm was observed besides the typical concentration peak for radii <1 µm (Deshler et al., 1993) and typically associated with coarse ash particles. For the Hunga Tonga aerosol plume, LOAC observations (measuring aerosol particles up to 30 µm) reveal the absence of such a second mode, that is, plume particles radii exclusively remain below ∼1 µm (Figures 3a and 3b for the flights on 23 January and 26 January, respectively). Such a monomodal feature has already been observed for example, for the Sarychev and Calbuco volcanic plumes from 2009 to 2015, respectively (Bègue et al., 2017; Lurton et al., 2018; Zhu et al., 2018).

LOAC typology particle classifications (optically absorbing, semi-transparent, transparent, liquid or ice particles) at the selected plume altitudes (as indicated in Figure 2) for the in situ observations are summarized in Table 1 (and visualized in more detail in Figure S3 in Supporting Information S1). For both measurement flights the aerosol plume forms a distinct layer of partly absorbing, semi-transparent particles for aerosol radii <0.5 µm, and transparent, liquid particles for aerosol radii between 0.5 and 1.0 µm, at lower altitudes (around 22 km). The upper aerosol plume at 25 km altitude, measured on 23 January shows a distinct layer of transparent (<0.5 µm) and liquid (0.5–1.0 µm) particles. Aerosols at altitude levels outside the plumes (as defined in Figures 2 and S2 in

Table 1
Aerosol Typology Within the Hunga Tonga Plume at the Altitude Levels as Defined in Figure 2 and Figure S2 in Supporting Information S1

Flight	Particle size range	Typology
23rd January	<0.5 μm	Transparent, semi-transparent and absorbing
lower peak (~22 km)	0.5–1.0 μm	Liquid
23rd January	<0.5 μm	Semi-transparent
upper peak (~25 km)	0.5–1.0 μm	Transparent
26th January	<0.5 μm	Absorbing, semi-transparent and transparent
	0.5–1.0 μm	Transparent and liquid

Note. The complete aerosol typology information on all altitude levels are given in Figure S3 in Supporting Information S1.

Supporting Information S1) are purely identified as liquid aerosol particles by the LOAC typology retrieval. It is important to note that the partly absorbing component of the lower layer (~22 km) is associated with small particles (<0.5 μm) and therefore not dominant (i.e., in the extinction signal) compared to the non-absorbing component of larger particles (>0.5 μm). This can explain why absorbing aerosols are not observed by satellites with reduced sensitivity to small particles. Furthermore, Legras et al. (2022) show with HIMAWARI and CALIOP observations that no absorbing/ash component is detected a few days after the UTLS injection of the plume (due to fast sedimentation and condensation with sulfuric acid and water). Finally, during both LOAC measurement flights ice particles were not identified.

4. Discussion

Based on LOAC plume observations on aerosol size distribution, concentration, and typology analysis we present possible aerosol compositions for the sampled Hunga Tonga plume.

One first overarching remark is that the Hunga Tonga plume exhibits very different microphysical features compared to the Pinatubo eruption of 1991, as well as more recent moderate stratospheric eruptions like Raikoke 2019 (Kloss et al., 2021), with a completely absent coarse ash aerosol mode. The Hunga Tonga plume (1–2 weeks after its eruption) is composed of very small particles. For all analyzed plume altitudes, the LOAC typology analysis consistently identifies liquid and transparent particles for particles of the size range 0.5–1.0 μm. This points to the dominance of SA droplets within the plume. Sulfate aerosols are also consistently detected with satellite products (e.g., IMS/IASI SA optical depth). However, for all measured plumes (except 23/01 at 25 km altitude) the LOAC typology classification for particles with radii <0.5 μm identifies absorbing and semi-transparent particles. This could point to partially small sulfate-coated ash particles or a thin, separated layer of ash below a layer of SA particles, with a vertical extent too thin to be identified as a separate layer by LOAC and space-borne observations. Such an ash-SA altitude separation was observed in Vernier et al. (2016) following the Kelud eruption in 2014. Lab experiments show that even a small ratio of ash to sulfuric acid can produce optically absorbing particles. Hence, the identification of absorbing particles does not necessarily point to a composition dominated by ash. The absorbing particles observed by LOAC are exceptionally small (<0.5 μm). For example, 3 months after the Kelud eruption ash particles with radii exclusively above 0.5 μm were observed (Vernier et al., 2016). The exceptionally small ash particles in the Hunga Tonga plume could have originated from the particular eruption dynamics (magma-seawater interaction, Wylie et al. (1999) and Yuen et al. (2022), with the inherent production of particularly small ash particles originating from the phreatomagmatic nature of the underwater Hunga Tonga eruption. The fact that satellite observations completely miss the small absorbing component of the sampled aerosol plume (based on Legras et al. (2022) and satellite observations presented in this study) shows how valuable and important it is to not only rely on global-space-borne observations, but also to consider highly sensitive in situ observations with better spatial resolution. Altogether, the observed absorbing component is not expected to have a significant impact on the larger scale optical/radiative properties of the plume.

The specific nature of the underwater eruption has produced record-breaking high stratospheric concentrations of water vapor with strong implications on aerosol formation and the stratospheric chemistry (Sellitto et al., 2022; Zhu et al., 2022). First results with the Microwave Limb Sounder and radio-sounding observations show the

injection of exceptionally large water content into the stratosphere during the Hunga Tonga eruption (Legras et al., 2022).

The plume measured at 25 km altitude on 23/01 shows a different composition compared to the plumes observed at 22 km. Particles of both size classes have a higher tendency toward optically transparent particles. This could point to a layer of predominant sulfate particles, clearly separating the plumes in terms of altitude and optical properties.

Overall, this study provides necessary, high resolution, complementary information to the existing and future studies on the microphysical properties of the plume, based on space-borne observations.

Data Availability Statement

LOAC in situ observations can be accessed from https://zenodo.org/record/6522689#.YrBjAd869hE. LiO3 observations are available at https://geosur.osureunion.fr/geonetwork/srv/fre/catalog.search#/metadata/f2c35798-47b7-433c-8927-46cf7babca83. For the access of the OMPS v 2.0 data are available at https://disc.gsfc.nasa.gov/datasets/OMPS_NPP_LP_L2_AER_DAILY_2/summary (NASA EarthData registration required). CALIOP and MSG-1 data are available at https://www.icare.univ-lille.fr/asd-content/archive/?dir=CALIOP/ and https://www.icare.univ-lille.fr/asd-content/archive/?dir=GEO/MSG+0415/L1_B/ (Free instantaneous registration on icare is required https://www.icare.univ-lille.fr/asd-content/register).

Acknowledgments
This study was supported by Le laboratoire d'excellence VOLTAIRE (VOLatils—Terre, Atmosphère et Interactions—Resources et Environnement; ANR-10-LABX-100-01) and the ANR ASTUS (ANR-21-CE01-0007-01). The authors acknowledge the European Communities, the Région Réunion, CNRS, and Université de la Réunion for their support and contributions in the construction phase of the research infrastructure OPAR (Observatoire de Physique de l'Atmosphère de La Réunion). OPAR is presently funded by CNRS (INSU), Météo France and Université de La Réunion and managed by OSU-R (Observatoire des Sciences de l'Univers de La Réunion, UAR 3365). The authors thank the University of Reunion Island for the funding of the LOAC sondes. We would furthermore like to thank the whole scientific and technical team at OPAR responsible for LiDAR observations and help with LOAC balloon launches. We are grateful for the fast administrational arrangements at CNRS and University d'Orléans for the spontaneous campaign. Brian Kerridge at RAL is acknowledged for his help with the IMS product. We thank Virginie Lancelot and the OSUC-team for fast administrational realization of the financement and travel logistics.

References

Baray, J.-L., Courcoux, Y., Keckhut, P., Portafaix, T., Tulet, P., Cammas, J.-P., et al. (2013). Maïdo Observatory: A new high-altitude station facility at Reunion Island (21°S, 55°E) for long-term atmospheric remote sensing and in situ measurements. *Atmospheric Measurement Techniques*, *6*(10), 2865–2877. https://doi.org/10.5194/amt-6-2865-2013

Bègue, N., Vignelles, D., Berthet, G., Portafaix, T., Payen, G., Jégou, F., et al. (2017). Long-range transport of stratospheric aerosols in the Southern Hemisphere following the 2015 Calbuco eruption. *Atmospheric Chemistry and Physics*, *17*(24), 15019–15036. https://doi.org/10.5194/acp-17-15019-2017

Carr, J. L., Horváth, k., Wu, D. L., & Friberg, M. D. (2022). Stereo plume height and Motion retrievals for the record-setting Hunga Tonga-Hunga Ha'apai eruption of 15 January 2022. *Geophysical Research Letters*, *49*(9), e2022GL098131. https://doi.org/10.1029/2022gl098131

Chazette, P., David, C., Lefrère, J., Godin, S., Pelon, J., & Mégie, G. (1995). Comparative lidar study of the optical, geometrical, and dynamical properties of stratospheric post-volcanic aerosols, following the eruptions of El Chichon and Mount Pinatubo. *Journal of Geophysical Research*, *100*(D11), 23195–23207. https://doi.org/10.1029/95jd02268

Clerbaux, C., Boynard, A., Clarisse, L., George, M., Hadji-Lazaro, J., Herbin, H., et al. (2009). Monitoring of atmospheric composition using the thermal infrared IASI/MetOp sounder. *Atmospheric Chemistry and Physics*, *9*(16), 6041–6054. https://doi.org/10.5194/acp-9-6041-2009

Da, C. (2015). Preliminary assessment of the Advanced Himawari Imager (AHI) measurement onboard Himawari-8 geostationary satellite. *Remote Sensing Letters*, *6*(8), 637–646. https://doi.org/10.1080/2150704X.2015.1066522

Deshler, T., Johnson, B. J., & Rozier, W. R. (1993). Balloonborne measurements of Pinatubo aerosol during 1991 and 1992 at 41°N: Vertical profiles, size distribution, and volatility. *Geophysical Research Letters*, *20*(14), 1435–1438. https://doi.org/10.1029/93gl01337

Dieudonné, E., Chazette, P., Marnas, F., Totems, J., & Shang, X. (2015). Lidar profiling of aerosol optical properties from Paris to Lake Baikal (Siberia). *Atmospheric Chemistry and Physics*, *15*(9), 5007–5026. https://doi.org/10.5194/acp-15-5007-2015

Duflot, V., Baray, J.-L., Payen, G., Marquestaut, N., Posny, F., Metzger, J.-M., et al. (2017). Tropospheric ozone profiles by DIAL at Maïdo observatory (Reunion Island): System description, instrumental performance and result comparison with ozone external data set. *Atmospheric Measurement Techniques*, *10*(9), 3359–3373. https://doi.org/10.5194/amt-10-3359-2017

Eumetrain (2020). EUMeTrain quick guides. Retrieved from https://resources.eumetrain.org/rgb_quick_guides/index.html

Klett, J. D. (1985). Lidar inversion with variable backscatter/extinction ratios. *Applied Optics*, *24*(11), 1638–1643. https://doi.org/10.1364/ao.24.001638

Kloss, C., Berthet, G., Sellitto, P., Ploeger, F., Taha, G., Tidiga, M., et al. (2021). Stratospheric aerosol layer perturbation caused by the 2019 Raikoke and Ulawun eruptions and their radiative forcing. *Atmospheric Chemistry and Physics*, *21*(1), 535–560. https://doi.org/10.5194/acp-21-535-2021

Legras, B., Duchamp, C., Sellitto, P., Podglajen, A., Carboni, E., Siddans, R., et al. (2022). The evolution and dynamics of the Hunga Tonga plume in the stratosphere. *EGUsphere*, 1–19. Preprint. https://doi.org/10.5194/egusphere-2022-517

Lurton, T., Jégou, F., Berthet, G., Renard, J.-B., Clarisse, L., Schmidt, A., et al. (2018). Model simulations of the chemical and aerosol microphysical evolution of the Sarychev Peak 2009 eruption cloud compared to in situ and satellite observations. *Atmospheric Chemistry and Physics*, *18*(5), 3223–3247. https://doi.org/10.5194/acp-18-3223-2018

Prata, A. T., Young, S. A., Siems, S. T., & Manton, M. J. (2017). Lidar ratios of stratospheric volcanic ash and sulfate aerosols retrieved from CALIOP measurements. *Atmospheric Chemistry and Physics*, *17*(13), 8599–8618. https://doi.org/10.5194/acp-17-8599-2017

Proud, S. R., Prata, A., & Schmauss, S. (2022). The January 2022 eruption of Hunga Tonga-Hunga Ha'apai volcano reached the mesosphere. *Earth and Space Science Open Archive*, *11*. Preprint. https://doi.org/10.1002/essoar.10511092.1

Renard, J.-B., Berthet, G., Levasseur-Regourd, A.-C., Beresnev, S., Miffre, A., Rairoux, P., et al. (2020). Origins and spatial distribution of non-pure sulfate particles (nsps) in the stratosphere detected by the balloon-borne light optical aerosols counter (LOAC). *Atmosphere*, *11*(10), 1031. https://doi.org/10.3390/atmos11101031

Renard, J.-B., Dulac, F., Berthet, G., Lurton, T., Vignelles, D., Jégou, F., et al. (2016). LOAC: A small aerosol optical counter/sizer for ground-based and balloon measurements of the size distribution and nature of atmospheric particles—Part 1: Principle of measurements and instrument evaluation. *Atmospheric Measurement Techniques*, *9*(4), 1721–1742. https://doi.org/10.5194/amt-9-1721-2016

Renard, J.-B., Michoud, V., & Giacomoni, J. (2020). Vertical profiles of pollution particle concentrations in the boundary layer above Paris (France) from the optical aerosol counter LOAC onboard a touristic balloon. *Sensors*, *20*(4), 1111. https://doi.org/10.3390/s20041111

Saunders, R., Hocking, J., Rundle, D., Rayer, P., Hayemann, S., Matricardi, A., et al. (2017). RTTOV-12 science and validation report; Version: 1.0. Doc ID: NWPSAF-MO-TV-41(D2.2).

Sellitto, P., & Legras, B. (2016). Sensitivity of thermal infrared nadir instruments to the chemical and microphysical properties of UTLS secondary sulfate aerosols. *Atmospheric Measurement Techniques*, *9*(1), 115–132. https://doi.org/10.5194/amt-9-115-2016

Sellitto, P., Podglajen, A., Belhadji, R., Boichu, M., Carboni, E., Cuesta, J., et al. (2022). The unexpected radiative impact of the Hunga Tonga eruption of January 15th, 2022, 18 April 2022, Preprint (Version 1) available at Research Square. https://doi.org/10.21203/rs.3.rs-1562573/v1

Sellitto, P., Sèze, G., & Legras, B. (2017). Secondary sulphate aerosols and cirrus clouds detection with Seviri during Nabro volcano eruption. *International Journal of Remote Sensing*, *38*(20), 5657–5672. https://doi.org/10.1080/01431161.2017.1348635

Siddans, R. (2019). Water vapour climate change initiative (WV CCI) phase one, deliverable 2.2; Version 1.0. STFC Rutherford Appleton Laboratory (RAL)(D2.2). Retrieved from https://climate.esa.int/documents/1337/Water_Vapour_CCI_D2.2_ATBD_Part2-IMS_L2_product_v1.0.pdf

Vernier, J.-P., Fairlie, T. D., Deshler, T., Natarajan, M., Knepp, T., Foster, K., et al. (2016). In situ and space-based observations of the Kelud volcanic plume: The persistence of ash in the lower stratosphere. *Journal of Geophysical Research: Atmospheres*, *121*(18), 11104–11118. https://doi.org/10.1002/2016jd025344

Witze, A. (2022). Why the Tongan eruption will go down in the history of volcanology. *Nature*, 376–378. https://doi.org/10.1038/d41586-022-00394-y

Wylie, J. J., Voight, B., & Whitehead, J. A. (1999). Instability of magma flow from volatile-dependent viscosity. *Science*, *285*(5435), 1883–1885. https://doi.org/10.1126/science.285.5435.1883

Yuen, D. A., Scruggs, M. A., Spera, F. J., Zheng, Y., Hu, H., McNutt, S. R., et al. (2022). Under the surface: Pressure-induced planetary-scale waves, volcanic lightning, and gaseous clouds caused by the submarine eruption of Hunga Tonga-Hunga Ha'apai volcano. *Earthquake Research Advances*, *2*(3), 100134. https://doi.org/10.1016/j.eqrea.2022.100134

Zhu, Y., Bardeen, C., Tilmes, S., Mills, M., Harvey, V., Taha, G., et al. (2022). 2022 Hunga-Tonga eruption: Stratospheric aerosol evolution in a water-rich plume. Preprint (Version 1) available at Research Square. https://doi.org/10.21203/rs.3.rs-1647643/v1

Zhu, Y., Toon, O. B., Kinnison, D., Harvey, V. L., Mills, M. J., Bardeen, C. G., et al. (2018). Stratospheric aerosols, polar stratospheric clouds, and polar ozone depletion after the mount Calbuco eruption in 2015. *Journal of Geophysical Research: Atmospheres*, *123*(21), 12308–12331. https://doi.org/10.1029/2018jd028974